



UNIVERSITY OF LEEDS

This is a repository copy of *Electrical and radiation characteristics of semilarge photoconductive terahertz emitters*.

White Rose Research Online URL for this paper:  
<http://eprints.whiterose.ac.uk/720/>

---

**Article:**

Stone, M.R., Naftaly, M., Miles, R.E. et al. (2 more authors) (2004) Electrical and radiation characteristics of semilarge photoconductive terahertz emitters. *IEEE Transactions on Microwave Theory and Techniques*, 52 (10). pp. 2420-2429. ISSN 0018-9480

<https://doi.org/10.1109/TMTT.2004.835980>

---

**Reuse**

See Attached

**Takedown**

If you consider content in White Rose Research Online to be in breach of UK law, please notify us by emailing [eprints@whiterose.ac.uk](mailto:eprints@whiterose.ac.uk) including the URL of the record and the reason for the withdrawal request.



[eprints@whiterose.ac.uk](mailto:eprints@whiterose.ac.uk)  
<https://eprints.whiterose.ac.uk/>

# Electrical and Radiation Characteristics of Semilarge Photoconductive Terahertz Emitters

Michael R. Stone, *Student Member, IEEE*, Mira Naftaly, Robert E. Miles, *Member, IEEE*, John R. Fletcher, and David Paul Steenson, *Senior Member, IEEE*

**Abstract**—We present experimental characterization of semilarge photoconductive emitters, including their electrical/photoconductive parameters and terahertz spectra. A range of emitters were studied and fabricated on both LT-GaAs and SI-GaAs, having a variety of electrode geometries. The spatial cone of terahertz radiation was defined. The dependencies of the photocurrent and the terahertz power on the bias voltage and the laser power were determined. A Fourier-transform interferometer is used to determine the terahertz spectra and to clarify the effects of the substrate and electrode geometry.

**Index Terms**—Interferometer, low-temperature (LT) grown GaAs, photoconductive emitter, terahertz.

## I. INTRODUCTION

TECHNIQUES OF generating terahertz radiation have been extensively studied and employed over the past 30 years. The most commonly used methods are optical rectification in nonlinear crystals [1]–[3] and ultrafast switching of biased photoconductive emitters [3]–[10].

Biased photoconductive emitters are fabricated by depositing two shaped electrodes on semiconductor wafers, typically low-temperature (LT) or semiinsulating (SI) GaAs. The emitter is switched by ultrashort laser pulses creating photocarriers in the semiconductor. The power for terahertz generation is provided by a dc-bias voltage applied to the electrodes. The bias field causes the photocarriers to accelerate, whereby they emit high-frequency radiation. The choice of substrate is dictated by the requirement for a short recombination time, which is  $\sim 100$  ps for SI GaAs and less than 1 ps for LT GaAs [8], [9]. Moreover, LT GaAs has the advantage of low carrier mobility, resulting in low photocurrent and, therefore, less heating. In order to excite carriers, the energy of the pump laser photons must exceed the energy gap of the semiconductor. The laser pulsewidth must be as narrow as possible to enable high-frequency radiation to be produced. Typically, photoconductive sources are switched by mode-locked Ti-sapphire lasers with pulse lengths of 10–100 fs operating at around 800 nm. The intensity, spectrum, and spatial distribution of emitted radiation depend on

the photoconductive substrate, electrode geometry and gap size, and bias field [9]–[12]. Two broad types of biased photoconductive emitters have been studied: narrow-gap, with the gap size of  $\sim 5$ – $50$   $\mu\text{m}$  [5], [7], [9], and large gap, with the gap size of  $\sim 0.1$ – $5$  mm [3], [6]. Unlike conventional microwave antennas, which are driven at a single frequency, photoconductive sources can generate radiation over a broad frequency spectrum. However, the electrode structure can act as a filter determining the radiated frequency spectrum. This applies particularly to narrow-gap emitters [7]–[10].

Semilarge emitters have the advantage of simplified fabrication. Moreover, it is possible to deposit electrodes of sufficient thickness to accommodate the skin depth and also to reduce the heating effects. Biased emitters with contacts formed by silver epoxy have been reported to produce 40  $\mu\text{W}$  of terahertz power with a bandwidth of 6 THz [16]. Semilarge structures offer a good compromise in properties and performance between microscopically small ( $< 100$   $\mu\text{m}$ ) and millimeter-size structures ( $> 1$  mm). Although the achievable bandwidth is narrower than that from microstructured antennas, the spectral characteristics are less dependent upon the emitter geometry, and unlike as in large-gap sources, high terahertz powers can be produced using unamplified mode-locked femtosecond lasers.

We have studied the properties of semilarge biased photoconductive emitters fabricated on both SI and LT GaAs and having a variety of electrode geometries. The directivity of the source was determined by measuring the spatial distribution of the emitted radiation. The dependence of the photocurrent on the bias voltage and laser power was investigated, as was the relationship between the emitted terahertz power and the photocurrent and laser power. A novel Fourier-transform terahertz interferometer was used to measure the spectra produced by the different sources. These spectra were related to the substrate and electrode geometry.

## II. EXPERIMENTAL SETUP

The photoconductive emitters used in the experiment were fabricated using standard microstructure processing. Both the SI and LT GaAs wafers were approximately 0.4-mm thick and polished on both sides. Electrical contacts were formed on the substrates using standard photolithography techniques. An adhesion layer of approximately 10 nm of Cr and an electrode layer of approximately 300 nm of Au were deposited. The electrode structures were all designed with semilarge apertures of between 0.1–2 mm, and with varying electrode lengths, widths,

Manuscript received May 2, 2003; revised June 25, 2004. This work was supported in part by the U.K. Research Council under Basic Technology Research Grant GR/R88106/01, by the Engineering and Physical Science Research Council under Joint Infrastructure Fund GM/M87535/01, by the Paul Instrument Fund (PIF) under PIF/GECL, by Teravision, and by the Engineering and Physical Sciences Research Council under a studentship.

The authors are with the Institute of Microwave and Photonics, School of Electronic and Electrical Engineering, The University of Leeds, Leeds LS2 9JT, U.K. (e-mail: eenmrs@leeds.ac.uk; M.Naftaly@leeds.ac.uk; r.e.miles@leeds.ac.uk; JohnFletcher@lenton9.fsnet.co.uk; d.p.steenson@leeds.ac.uk).

Digital Object Identifier 10.1109/TMTT.2004.835980

TABLE I  
PROPERTIES OF SEMIINSULATING AND LOW-TEMPERATURE-GROWN  
GaAs SUBSTRATES

Material	Effective carrier lifetime	Breakdown field	Electron mobility
Semi-insulating GaAs	~ 1ns [13]	~4·10 <sup>5</sup> V/cm	8500 cm <sup>2</sup> /Vs
Low-temperature GaAs	< 1ps [14,15]	>4·10 <sup>5</sup> V/cm	200 cm <sup>2</sup> /Vs

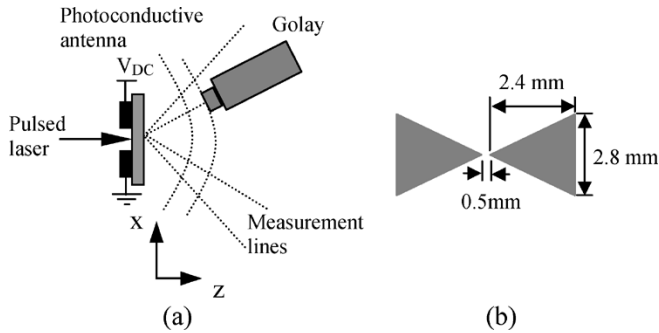


Fig. 1. (a) Schematic diagram of the setup for the measurement of the spatial cone of terahertz radiation from a biased emitter. (b) Electrode structure of the semilarge biased emitter used in the experiments.

and shapes. The applied dc voltage varied between 30–350 V, depending on the type of substrate and size of the gap. The photoconductive substrates used were chosen for their well-known properties and tradeoffs, as shown in Table I [13]–[15].

All the emitters were mounted on large copper electrodes and contacted using standard silver epoxy. The large electrodes were employed to help dissipate the heat generated by the photocurrent. Cooling has been reported to produce an overall increase in terahertz power generated by this type of emitter [16].

The emitters were activated by a mode-locked Ti-sapphire laser (MaiTai, Spectra-Physics, Mountain View, CA) with a pulsewidth of ~80 fs and an average power of 1.1 W. The laser was set to operate at 800 nm, which is above the absorption edge of GaAs at ~880 nm. It was found that the emitted terahertz power was maximized when the laser beam was directed at the center of the gap between the electrodes and was focused to a beam spot slightly smaller than the gap size.

The radiation emitted by the photoconverter was detected by a Golay cell (Type OAD-7, QMC Instruments, Cardiff, U.K.), whose sensitivity range extended over 3–650 cm<sup>-1</sup> (0.1–20 THz) and whose aperture was 6 mm. To ensure that only terahertz radiation was registered by the Golay detector, an Si wafer was placed at its input as a blocking filter. The signal from the Golay was recovered using a lock-in amplifier (Model 7265, EG&G Instruments, Gaithersburg, MD). The laser beam was mechanically chopped at 11 Hz in order to accommodate the slow response time of the Golay and to operate within its optimum SNR regime.

Fig. 1(a) depicts the setup used for the measurement of emitter directivity. Fig. 1(b) shows the size and geometry of the bias electrodes used in this experiment. For this measurement, the Golay cell was moved horizontally away from the antenna along lines set at fixed angles relative to the antenna plane. By repeating the measurement at different angles over a range of

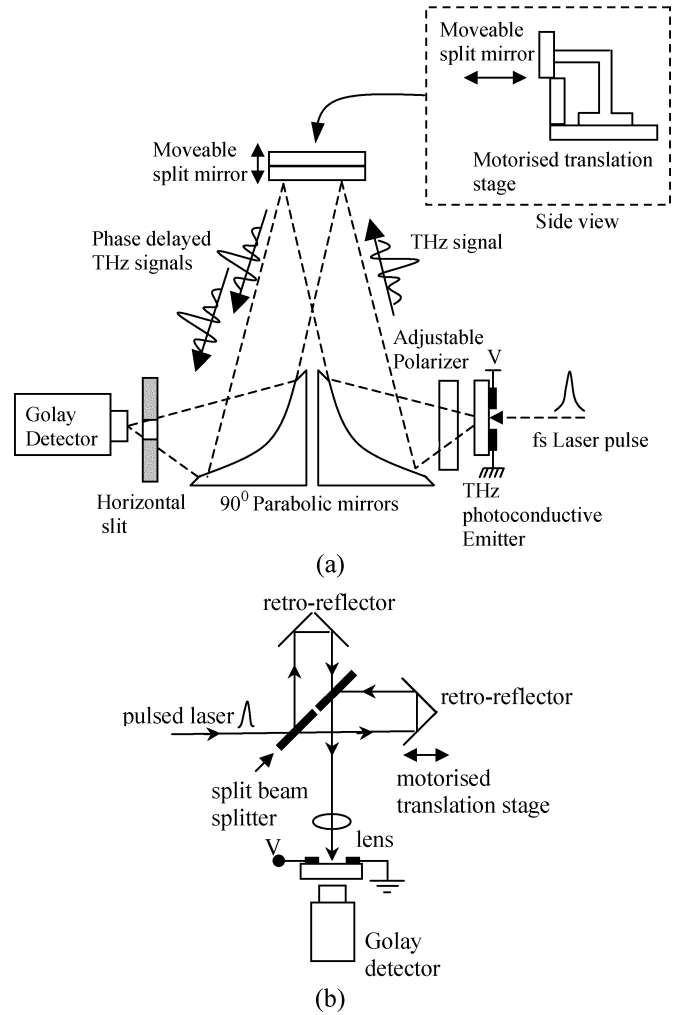


Fig. 2. Schematic diagrams of: (a) the Fourier-transform terahertz interferometer and (b) the autocorrelator setup.

distances, the spatial distribution of the emitted radiation was mapped out.

The dependence of the emitted terahertz power on the bias voltage and laser power was measured by placing the Golay cell directly behind and parallel to the source at a distance of approximately 10 mm. The average photocurrent was measured by inserting an ammeter into the bias circuit. For the laser power measurements, the beam incident on the source was attenuated by a variable neutral density filter while being monitored by a laser power meter.

The configuration of the Fourier-transform terahertz interferometer used to examine the frequency spectra of different biased emitters is shown in Fig. 2(a). The design and operation of the interferometer are described in [17]. The terahertz radiation is collected and collimated by a 2-in gold-coated off-axis parabolic mirror (90°, NA = 1). The collimated beam is directed onto a split mirror (shown in the insert), one-half of which is mounted on a motorized translation stage, and which divides the beam into two halves. The reflected beams are then directed onto the second parabolic mirror, which combines and focuses them to form an interference pattern in the focal plane. An interferogram is generated by scanning the top half of the split

mirror, producing a variable time delay and, therefore, a phase shift, between the two halves of the terahertz beam.

A horizontal slit is placed at the focal plane of the second parabolic mirror in order to increase the instrument sensitivity at higher frequencies and thereby widen the detection bandwidth. The terahertz radiation is detected by a Golay cell placed directly behind the slit and connected to a lock-in amplifier.

An alternative technique has been used in determining the terahertz spectrum produced by coherent plasmons in unbiased n-doped GaAs [18]. This method uses an autocorrelator configuration, with the terahertz emitter acting as a detector element, as shown in Fig. 2(b). The autocorrelator is a Michelson interferometer, which splits the laser beam and recombines it after a variable delay. The recombined beam, which carries the interference pattern, is incident on the emitter, causing variations in the intensity of the produced terahertz radiation detected by the Golay cell. We have investigated using this method to study the spectra of biased sources [19]. However, it was found that the results were radically different from those obtained by the terahertz interferometer and, furthermore, were inconsistent with the known performance of such emitters [16]. It was concluded, therefore, that the autocorrelation technique is unsuitable for biased emitters (see Section III-F).

### III. RESULTS AND DISCUSSIONS

All the experiments on the directivity of emitted terahertz radiation and the relationships between the bias voltage, photocurrent, laser power, and emitted terahertz power, which are described below, were carried out using biased sources having the electrode configuration shown in Fig. 1(b).

The results were analyzed in the light of the current surge model of terahertz generation in biased emitters [3], [20], [21]. For the sake of simplicity, we assume that the bias voltage remains approximately constant and that the effects of electrode geometry can be neglected. These assumptions are justified in our case because the laser power is insufficient to produce saturation, and because the emitters have relatively large apertures, reducing the geometrical effect of the electrodes. We further assume that the dark conductivity of GaAs is negligible. The transient photocurrent  $J(t)$  is then directly proportional to the induced photoconductivity of the material  $\sigma$  and the applied biased field  $E_{\text{bias}}$ , i.e.,

$$J(t) = \sigma(t)E_{\text{bias}}. \quad (1)$$

The photoconductivity  $\sigma(t)$  is, in turn, proportional to the carrier mobility and density

$$\sigma(t) = e\mu n(t). \quad (2)$$

Here,  $\mu$  is taken to be the electron mobility since the hole mobility is much lower [13] and can be neglected. Carriers are generated in the semiconductor by the incident laser pulse so that

$$n(t) = G_0 \int_{-\infty}^t g(t')e^{-\frac{(t-t')}{\tau_r}} dt' \quad (3)$$

where  $G_0$  is the absorbed photon density,  $g(t)$  is the temporal profile of the laser pulse, and  $\tau_r$  is the carrier recombination time. Although the pulse shape of an ideal mode-locked laser has a  $\text{sech}^2$  profile, a useful approximation can be obtained by assuming a square pulse shape such that

$$g(t) = \begin{cases} 1, & 0 < t < T_{\text{pulse}} \\ 0, & \text{elsewhere} \end{cases} \quad (4)$$

where  $T_{\text{pulse}}$  is the laser pulse length. The photocarrier density is then given by

$$n(t) = \begin{cases} G_0\tau_r \left(1 - e^{-\frac{t}{\tau_r}}\right), & 0 < t < T_{\text{pulse}} \\ G_0\tau_r e^{-\frac{t}{\tau_r}}, & T_{\text{pulse}} < t. \end{cases} \quad (5)$$

Thus, the average value of the carrier density is

$$\langle n \rangle = G_0 \frac{T_{\text{pulse}} + \tau_r \left(2e^{-\frac{T_{\text{pulse}}}{\tau_r}} - 1\right)}{\frac{T_{\text{rep}}}{\tau_r}} \quad (6)$$

where  $T_{\text{rep}}$  is the period between successive laser pulses. The average carrier density is seen to increase with the recombination lifetime  $\tau_r$ . The average photocurrent then becomes

$$\begin{aligned} \langle J \rangle &= \langle \sigma \rangle E_{\text{bias}} \\ &= e\mu E_{\text{bias}} \langle n \rangle \\ &= e\mu E_{\text{bias}} G_0 \frac{T_{\text{pulse}} + \tau_r \left(2e^{-\frac{T_{\text{pulse}}}{\tau_r}} - 1\right)}{\frac{T_{\text{rep}}}{\tau_r}} \end{aligned} \quad (7)$$

Terahertz radiation is emitted by accelerating carriers, producing a terahertz pulse according to

$$E_{\text{THz}}(t) \sim \frac{dJ(t)}{dt} \sim \frac{E_{\text{bias}} dn(t)}{dt} \quad (8)$$

and the resulting terahertz spectrum is given by the Fourier transform of the time-domain signal. The average terahertz power  $P_{\text{THz}}$  is the average of the square of the terahertz field

$$\begin{aligned} P_{\text{THz}} = \langle E_{\text{THz}}^2 \rangle &\sim \left\langle \left( \frac{dJ}{dt} \right)^2 \right\rangle \\ &\sim E_{\text{bias}}^2 \left\langle \left( \frac{dn}{dt} \right)^2 \right\rangle \sim \frac{E^2 G_0^2 \tau_r}{2T_{\text{rep}}}. \end{aligned} \quad (9)$$

The *average* terahertz power is, therefore, proportional to the square of both the applied field and laser power. It is also proportional to the recombination time. However, a long recombination time reduces both the *peak* terahertz power and the emission bandwidth and, therefore, is detrimental to terahertz generation.

#### A. Spatial Distribution of Emitted Radiation

Fig. 3(a) plots the angular dependence of the terahertz signal emitted by the source at different distances from its plane. It is seen that the signal is reduced to approximately half its peak intensity at an angle of  $\pm 20^\circ$  giving a radiation cone of  $\sim 40^\circ$ .

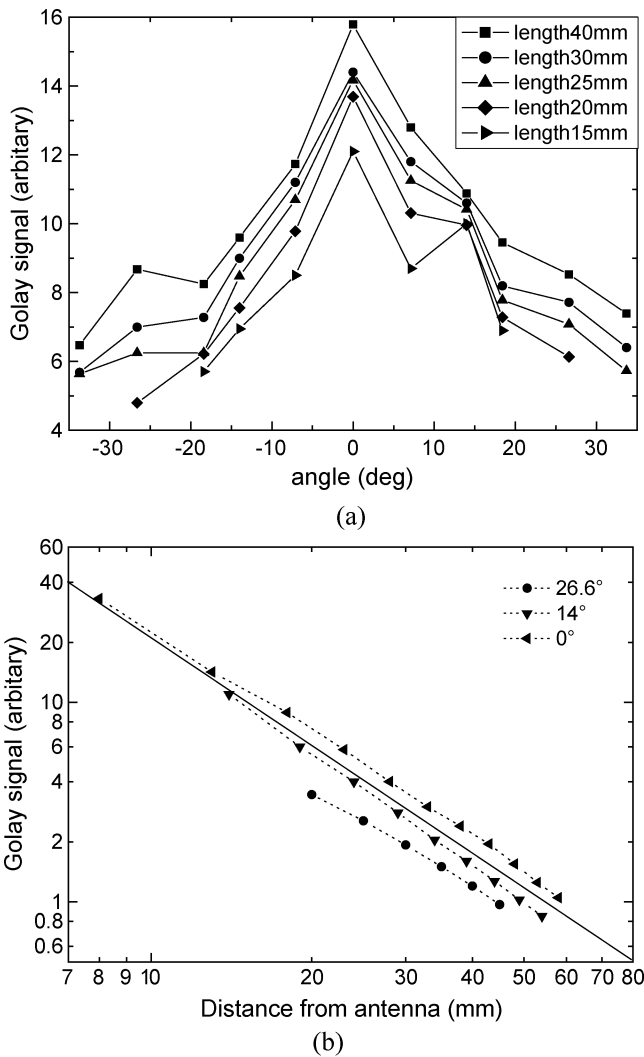


Fig. 3. (a) Angular distribution of the terahertz signal at different distances from the emitter plane. (b) Terahertz signal as a function of distance from the emitter at different angles to the emitter plane.

This is somewhat more strongly directional than would be expected in a purely Hertzian dipole antenna. The signal is slightly asymmetric, especially at larger angles, which may be due to an asymmetric field distribution within the source. The variation of the terahertz power with the distance from the source is shown in Fig. 3(b) and is seen to follow the expected  $1/r^2$  dependence.

### B. Photocurrent Dependence on Bias Voltage

The relationship between the photocurrent and applied bias voltage was measured at a range of laser powers, as shown in Fig. 4. The observed data sets for both SI and LT GaAs show a threshold behavior at low bias fields, but are approximately linear above. This indicates a nonohmic resistance component in the metal–semiconductor contact. This component is much greater in the LT GaAs due to the shorter recombination time, lower carrier mobility, and higher breakdown field. The field threshold decreases with increasing laser power as expected since the conductivity of the photoconductor rises as the population of photocarriers grows (2).

The roughly linear sections of the curves confirm that the conductivity remains approximately constant as the bias field in-

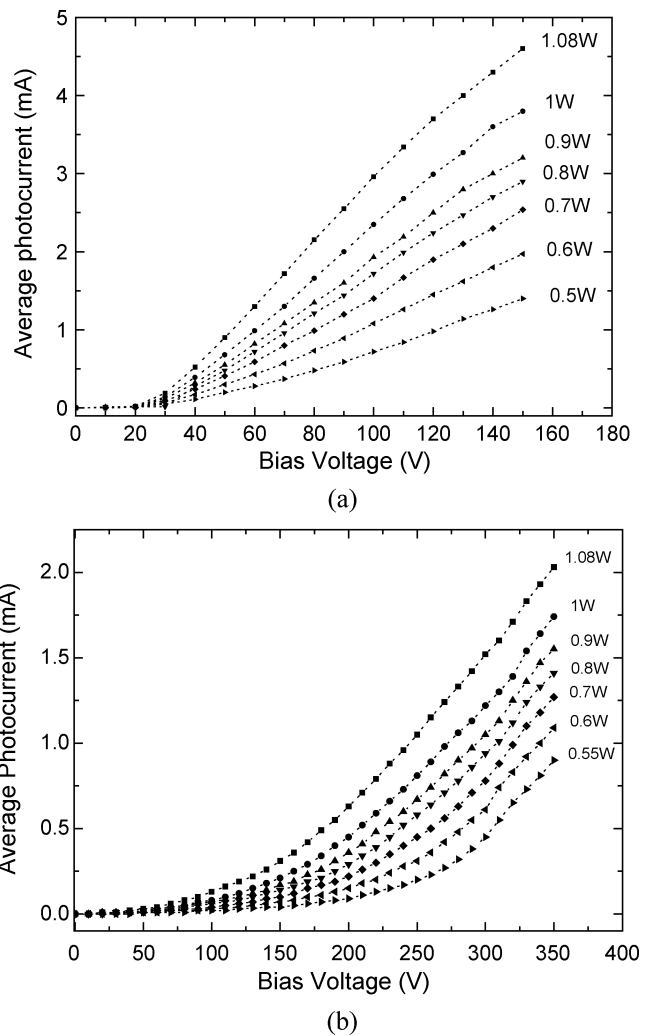


Fig. 4. Dependence of the photocurrent on the bias voltage for different laser powers. (a) SI GaAs. (b) LT GaAs.

creases [see (1) and (7)]. When the laser power is increased, the conductivity rises (indicated by the steeper slope) because more photocarriers are being created [see (2) and (6)]. This effect is observed more strongly in the SI GaAs due to the longer carrier lifetime (6). At lower laser powers, the incremental increase in conductivity between successive curves is roughly constant, confirming that conductivity is proportional to the incident optical power [see (2) and (6)]. However, at the higher laser power, the rise in conductivity is larger, possibly due to the heating of the semiconductor. Indeed, if the bias voltage continues to rise, the current starts to grow nonlinearly and a thermal runaway sets in. It was found that the threshold voltage at which thermal runaway occurs depends inversely on the laser power and emitter aperture [19]. In LT GaAs, the photocurrent remains much lower, reducing the ohmic heating and increasing the threshold voltage for thermal runaway. For this reason, it was possible to apply a higher bias voltage to LT GaAs than to SI GaAs.

### C. Photocurrent Dependence on Laser Power

The dependence of the photocurrent on the laser power at different bias voltages is seen in Fig. 5. Both substrates show very

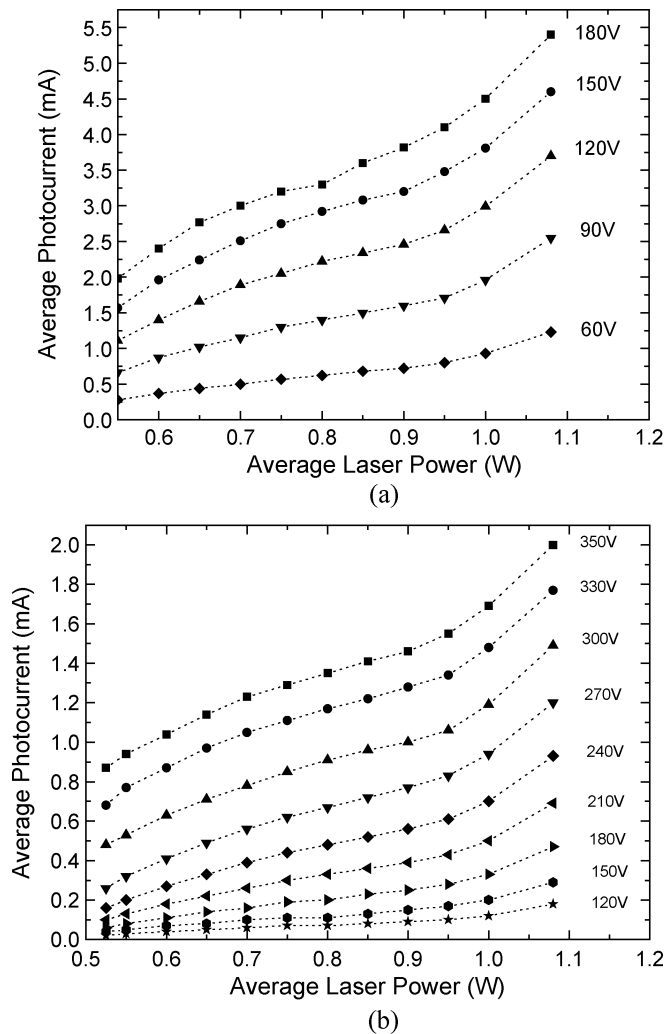


Fig. 5. Dependence of the emitter photocurrent on laser power for different bias voltages. (a) SI GaAs. (b) LT GaAs.

similar behavior, although LT GaAs generates a much lower current, as explained above. The curves are roughly linear, except at higher powers, confirming the relationship between conductivity and laser power [see (2) and (6)]. The slopes of the curves increase with applied bias since the average current is proportional to the field (7). At high optical powers, the current increases more steeply due to the heating of the substrate and the consequent increase in conductivity.

#### D. Dependence of Emitted Terahertz Power on Applied Bias Voltage

Fig. 6 shows the dependence of the emitted terahertz power on the bias voltage for different levels of optical power. Notably, both substrates produce similar terahertz power. This is despite higher bias being applied to LT GaAs, as shown in Figs. 4 and 5. The voltage threshold for terahertz generation, which is much higher in LT GaAs than in SI GaAs, corresponds to the similar threshold for photocurrent (Fig. 4) and confirms the relationship between photocurrent and terahertz emission (8).

In all cases, the relationship between the emitted terahertz power and applied bias voltage fits well to a square dependence,

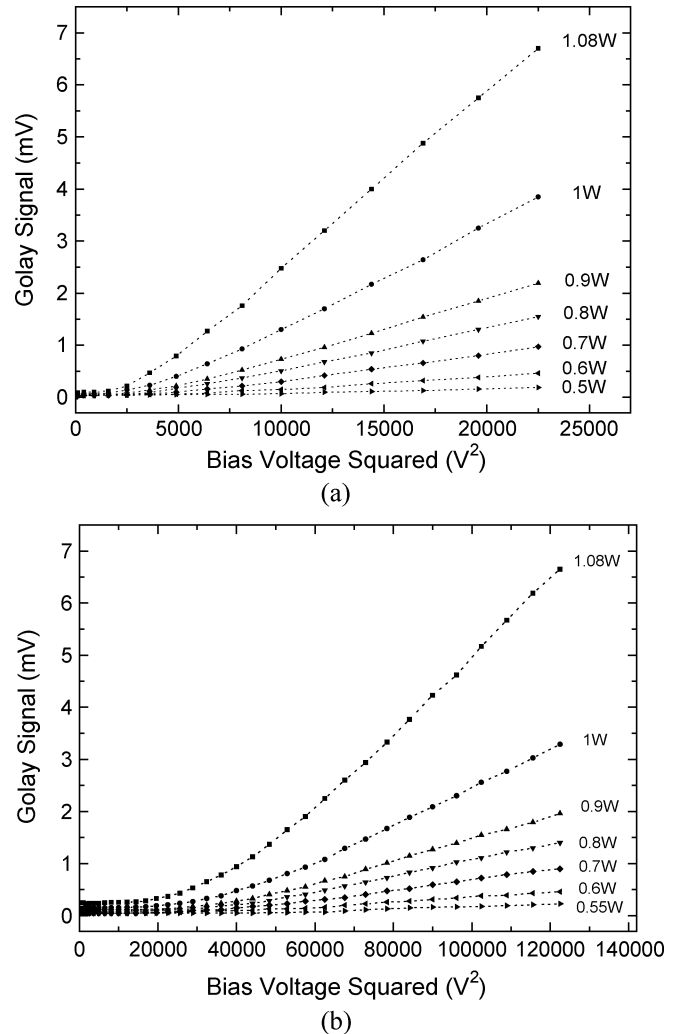


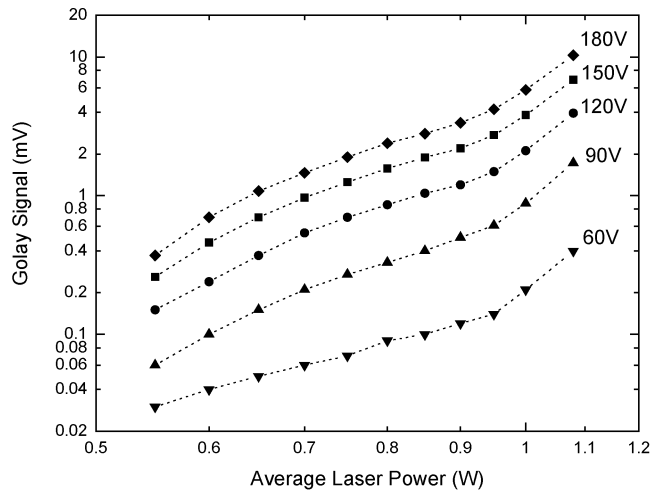
Fig. 6. Dependence of the average terahertz power on the square of the applied bias voltage for different laser power levels. (a) SI GaAs. (b) LT GaAs. Solid lines indicate  $x^2$  fits.

which is in agreement with (9). The steepness of the slopes increases with the laser power, reflecting the dependence on  $G_0^2$ . The effect of laser power is weaker in LT GaAs, i.e., the slopes increase less steeply, owing to the short recombination time (9).

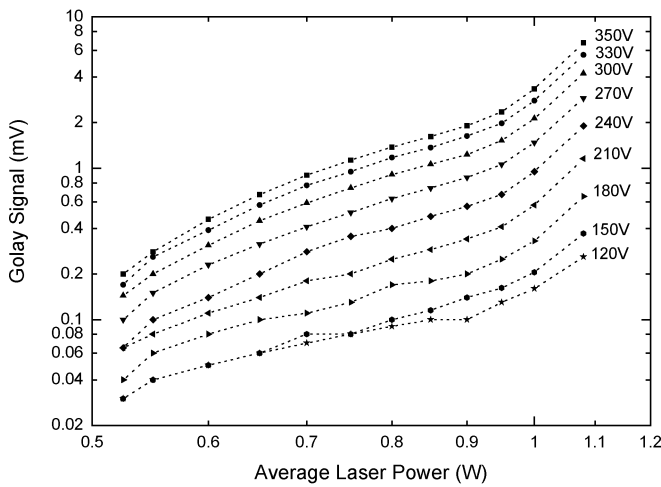
#### E. Dependence of Terahertz Power on Laser Power

Fig. 7 represents the dependence of the radiated terahertz power on the incident laser power. The data are derived from those in Figs. 4–6. The emitted terahertz power grows approximately as the square of the laser power, while also increasing with the applied bias voltage (Fig. 6). The rise in the terahertz power steepens at higher laser powers and high bias fields due to substrate heating, which increases conductivity [see (2), (7), and (8)]. For practical uses, it is, therefore, advantageous to operate at the maximum possible bias voltage and laser power.

However, the allowable bias voltage must remain below the electric breakdown value, and also below the threshold for thermal runaway. The usable laser power is limited by the optical saturation effects. These have been reported in systems using amplified lasers [3], [20]. In our experiments, saturation effects were not observed because the MaiTai laser does not



(a)



(b)

Fig. 7. Dependence of the average terahertz power on the average laser power for different bias voltages. (a) SI GaAs. (b) LT GaAs.

provide sufficiently high optical fluence when focused into a 0.5-mm aperture.

#### F. Terahertz Spectral Measurements

Terahertz spectra emitted by different biased sources fabricated on LT or SI GaAs were observed using the Fourier-transform terahertz interferometer. Fig. 8 shows a typical interferogram trace. The terahertz source, which generated this trace, was the same as used in all the above experiments and as shown in Fig. 1(b).

The central peak has a full width at half maximum (FWHM) of 0.9 ps and corresponds to the main terahertz signal. In addition, there are significant satellite peaks at  $\pm 11$  ps, which are due to reflections from the back of the SI-GaAs wafer. The nature of the satellite peaks is confirmed by considering the roundtrip time taken by the reflected pulse:  $t = 2dn/c \approx 11$  ps, where  $d = 450 \mu\text{m}$  is the thickness of the wafer,  $n \approx 3.6$  is the refractive index of GaAs, and  $c$  is the speed of light in vacuum. The height of the satellite peaks is  $\approx 10\%$  of the main peak height, which also agrees with the expected value for the attenuation. The fraction of power reflected at the air/GaAs interface arising from the difference in their refractive indices is

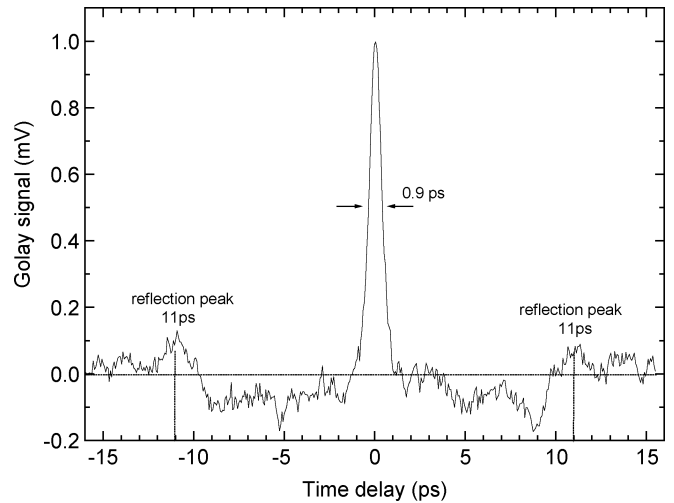


Fig. 8. Terahertz signal obtained by the interferometer from a triangular emitter fabricated on SI GaAs.

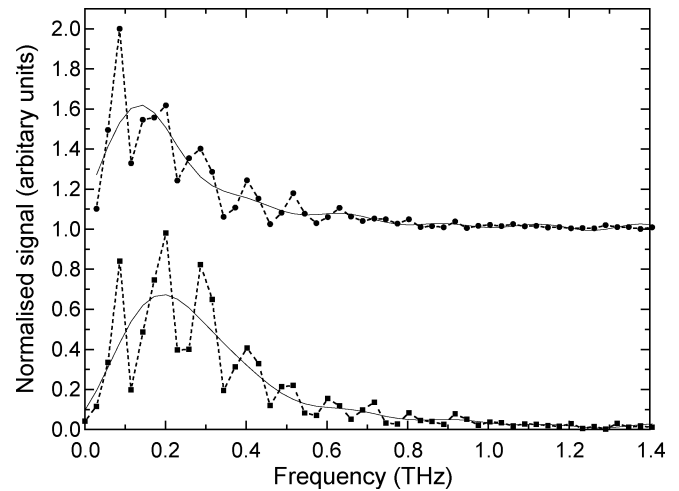


Fig. 9. Calculated terahertz spectra for two different electrode geometries (circles) and FFT filtered spectra (solid lines).

$R = (n - 1)^2/(n + 1)^2 \approx 0.32$ . The reflected beam undergoes two reflections (from the front and back surfaces) and one transmission (through the front surface), while the main beam experiences one transmission, giving the ratio between the two peak powers as  $R^2(1 - R)/(1 - R) \approx 0.1$ .

The emitted terahertz spectrum is calculated by applying the fast Fourier-transform (FFT) algorithm to the interferometer data. When using the FFT, the satellite peaks in the trace give rise to a spurious frequency component of  $f = (11 \text{ ps})^{-1} = 90 \text{ GHz}$ , which appears as oscillations in the spectrum, as shown in Fig. 9. These can be removed by applying an FFT filter to the calculated spectrum. The resulting spectra are plotted as solid curves in Fig. 9. For the sake of clarity, an FFT filter was applied to all spectra discussed below.

In initial experiments, reported in detail in [19], we attempted to measure the emitted terahertz spectra by using the autocorrelation technique employed elsewhere to observe spectra of unbiased plasmon emitters [18]. A typical trace, generated by the same source as in Fig. 8, is shown in Fig. 10. As explained above [see Fig. 2(b)], in this experiment, the laser beam travels

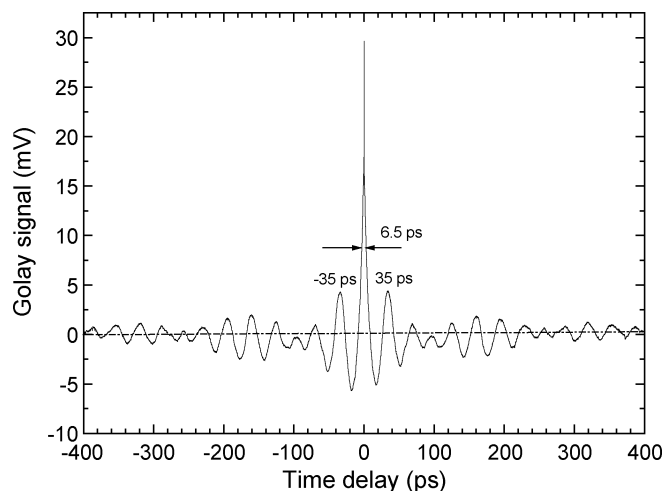


Fig. 10. Terahertz signal obtained by the autocorrelation method from a triangular emitter on SI GaAs.

through a Michelson interferometer and forms an interferogram on the emitter. The crucial difference between this setup and the terahertz interferometer is that, in the interferometer, the terahertz beam produced by the emitter is split and the two halves are made to interfere on the detector. By contrast, in the autocorrelator, the emitter experiences a varying incident beam containing two components, one of which arrives with a differential time delay.

It is seen that the two traces in Figs. 8 and 10 differ greatly. The oscillations in the autocorrelation trace extend for  $>300$  ps, which is two orders of magnitude longer than the terahertz pulse length expected from a biased source. The central peak has a FWHM of 6.5 ps compared to the 0.9 ps recorded by the terahertz interferometer. The discrepancy may be attributed to the fact that the autocorrelation method requires that the response of the emitter be linear and independent of the relative time delay between the two pulses. This is the case for plasmon emitters. However, it appears that biased emitters do not conform to these conditions. Indeed, the narrow spike at the center of the main peak can be resolved into an autocorrelation-like trace, indicating that the source response contains a square-dependence component, similar to a two-photon photodiode or a nonlinear crystal. In addition, interference fringes are seen to occur at 35-ps intervals in the trace, corresponding to a frequency of 30 GHz. These may be caused by parasitic oscillations in the transmission lines.

### G. Spectral Characteristics

Terahertz emission spectra were measured in a variety of biased sources, fabricated on LT or SI GaAs, and having different electrode geometries and gap sizes. Spectral characteristics were found to depend strongly on the substrate, and to a lesser extent on the gap size and electrode shape.

Equations (3) and (8) show that the spectral characteristics of a terahertz pulse are determined by the convolution of the laser pulse profile with the exponential decay of the carrier density. It follows that the terahertz bandwidth can be increased by reducing the laser pulse width or by using a semiconductor with a shorter carrier lifetime.

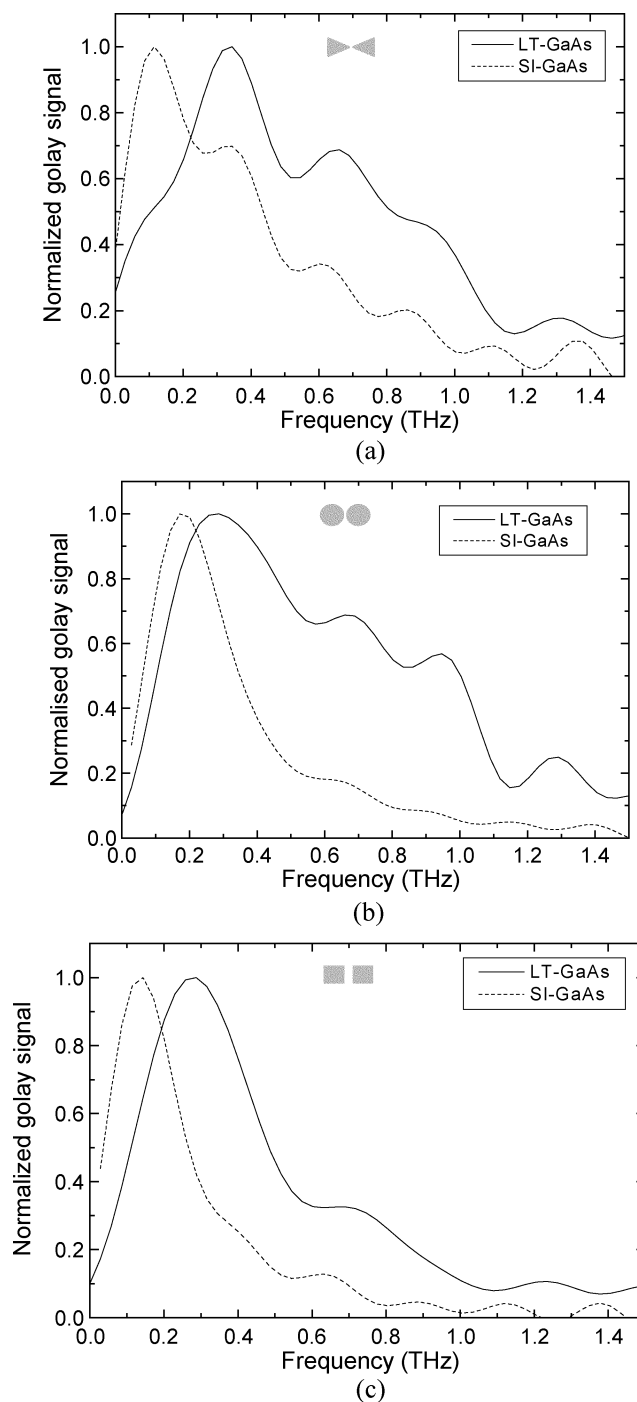


Fig. 11. Comparison of terahertz spectra from LT- and SI-GaAs emitters for three different electrode geometries. (a) Triangle. (b) Circle. (c) Square.

Terahertz radiation is generated within the semiconductor substrate. However, the electrodes generating the bias field have a strong influence on the terahertz near field and can, thus, affect both the spatial distribution and frequency spectrum in the far field. For small structures ( $<100$   $\mu\text{m}$ ), the electrodes act similarly to microwave antennas, as filtering and directional elements determined by their impedance. In large aperture sources ( $>1$  mm), the shape of the electrodes has a negligible effect, and the terahertz radiation produced in the semiconductor emerges co-linearly with the laser beam and is diffraction limited.

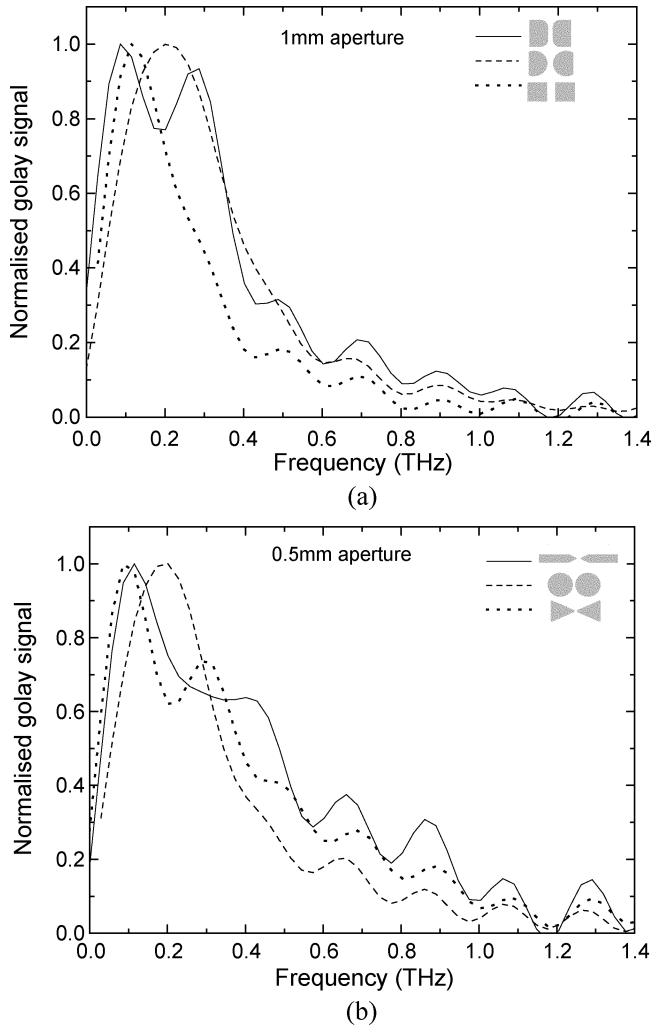


Fig. 12. Terahertz spectra obtained from SI-GaAs emitters with several different electrode geometries (shown in legends). (a) 1-mm gap. (b) 0.5-mm gap.

In the intermediate case of semilarge emitters considered here, the terahertz spectrum is determined primarily by the substrate, although the electrode structure also has an important effect. To check that terahertz radiation is produced in the semiconductor in agreement with the current surge model, the polarization of all sources was tested using a wire-grid polarizer. It was found that, in all cases, the terahertz radiation was polarized parallel to the applied bias field.

Fig. 11 demonstrates the effect of different electrode structures on the emitted terahertz spectrum. To investigate this further, a variety of electrodes were fabricated on SI GaAs. The spectra are compared in Fig. 12 and details relating to the electrode geometry and performance are given in Table II.

Several effects can be observed. First, smaller apertures give rise to significantly broader terahertz spectra extending to higher frequencies. However, it must be remembered that, as the aperture size decreases below the terahertz wavelength, the electrodes will begin to act as frequency filters. Second, higher fields, such as produced by more pointed electrodes, also contribute to somewhat broader spectra. This leads to the conclusion, indicated by (8), that for purposes of broad terahertz

TABLE II  
ELECTRODE GEOMETRIES AND DIMENSIONS, AND THE PEAKS AND BANDWIDTHS OF THE GENERATED TERAHERTZ SPECTRA

Electrode Geometries	Dimensions (mm)*	Peak (THz)*	FWHM (THz)*
	G=1, W=2, L=2	SI ~ 0.19	SI ~ 0.35
	G=1, W=2, L=2	SI ~ 0.086	SI ~ 0.2
	G=0.5, W=2, L=2	SI ~ 0.1	SI ~ 0.45
	G=0.5, W=3, L=3	LT ~ 0.35	LT ~ 0.8
	G=0.5, W=2, L=2	SI ~ 0.19	SI ~ 0.3
	G=1, W=2, L=2	LT ~ 0.28	LT ~ 0.9
	G=0.5, W=0.5, L=4	SI ~ 0.21	SI ~ 0.3
	G=0.5, W=0.5, L=4	SI ~ 0.12	SI ~ 0.37

emission, bias electrodes must be designed so as to produce a high electric field in the terahertz generating region. Notably, a rounded electrode profile, as in the circle and semicircle, shifts the spectrum to higher frequencies, but does not broaden it. Finally, square electrodes give rise to the narrowest spectrum at lowest frequencies. It may be concluded, therefore, that the preferred electrode structure will have a relatively small gap ( $\sim 0.5$  mm) and a fairly pointed profile.

#### IV. CONCLUSION

We have investigated terahertz generation in a variety of semilarge biased emitters fabricated on both LT and SI GaAs and having different electrode geometries. The behavior of these sources was seen to conform to the current surge model.

In practical applications, such as terahertz sources, the requirements are to maximize both the generated terahertz power and the emitted frequency bandwidth. It has been confirmed that the photocurrent is approximately linear with both bias voltage and laser power and, as a consequence, that the radiated terahertz power has an approximately square dependence on these parameters. However, to maintain high terahertz generation, it is necessary to avoid heating the semiconductor since that leads to thermal runaway. This restricts the bias and optical power that can be safely used without damaging the emitter to well below the levels at which electric breakdown or optical damage can occur. Applying cooling to the emitter has been shown to alleviate the problem [16].

LT GaAs was found to produce similar amounts of terahertz as SI GaAs at the same laser power, while generating a greatly reduced photocurrent. As a consequence, in LT GaAs, thermal runaway is delayed so that higher bias can be applied.

Terahertz spectra, measured using a Fourier transform interferometer, were found to be much broader in LT GaAs than in SI GaAs. Owing to its lower photocurrent and the ability to generate higher terahertz frequencies, LT GaAs is, therefore, the preferred substrate for biased emitters. However, unlike SI GaAs, individual wafers may vary significantly, affecting the reproducibility and reliability of performance.

Comparing terahertz spectra produced by emitters with different electrode geometries, it was seen that a high bias field

broadens the spectrum. The preferred electrode geometry, therefore, has a relatively narrow gap ( $\sim 0.5$  mm) and a pointed electrode profile.

#### ACKNOWLEDGMENT

The authors would like to thank E. Linfield and H. Beere for providing samples of LT GaAs (A2731) grown at Cavendish Laboratory, Cambridge, U.K. The authors would also like to thank V. Postoyalko, School of Electrical and Electronic Engineering, The University of Leeds, Leeds, U.K., for helpful discussions.

#### REFERENCES

- [1] B. B. Hu, X.-C. Zhang, D. H. Auston, and P. R. Smith, "Free space radiation from electro-optic crystal," *Appl. Phys. Lett.*, vol. 56, p. 506, 1990.
- [2] A. Rice, Y. Jin, X.-F. Ma, X.-C. Zhang, D. Bliss, J. Perkin, and M. Alexander, "Terahertz optical rectification from (110) zincblende crystals," *Appl. Phys. Lett.*, vol. 64, pp. 1324–1326, 1994.
- [3] X.-C. Zhang and Y. Jin, "Optically generated THz beams from dielectrics," in *Perspectives in Optoelectronics*, S. S. Jha, Ed, Singapore: World Scientific, 1995, ch. 3, pp. 81–138.
- [4] D. Mittleman, Ed., *Sensing With Terahertz Radiation*. ser. Opt. Sci. Berlin, Germany: Springer-Verlag, 2003, vol. 85.
- [5] M. Van Exter and D. R. Grischkowsky, "Characterization of an optoelectronic terahertz beam system," *IEEE Trans. Microwave Theory Tech.*, vol. 38, pp. 1684–1691, Nov. 1990.
- [6] A. J. Taylor, G. Rodriguez, and D. Some, "Ultrafast field dynamics in large-aperture photoconductors," *Opt. Lett.*, vol. 22, no. 10, pp. 715–717, May 1997.
- [7] P. R. Smith, D. H. Auston, and M. C. Nuss, "Subpicosecond photoconducting dipole antennas," *IEEE J. Quantum Electron.*, vol. 24, pp. 255–260, Feb. 1998.
- [8] Z. S. Piao, M. Tani, and K. Sakai, "Carrier dynamics and THz radiation in biased semiconductor structures," in *SPIE Terahertz Spectroscopy and Applications Conf.*, vol. 3617, San Jose, CA, Jan. 1999, pp. 49–56.
- [9] P. U. Jepsen, R. H. Jacobsen, and S. R. Keiding, "Generation and detection of terahertz pulses from biased semiconductor antennas," *J. Opt. Soc. Amer. B, Opt. Phys.*, vol. 13, no. 11, pp. 2424–2436, Nov. 1996.
- [10] J. V. Rudd, J. L. Johnson, and D. M. Mittleman, "Quadrupole radiation from terahertz dipole antennas," *Opt. Lett.*, vol. 25, no. 20, pp. 1556–1558, Oct. 15, 2000.
- [11] G. M. Rebeiz, "Millimeter-wave and terahertz circuit antennas," *Proc. IEEE*, vol. 80, pp. 1748–1770, Nov. 1992.
- [12] D. B. Rutledge, D. P. Neikirk, and D. P. Kasilingam, "Integrated-circuit antennas," in *Infrared Millim. Waves*, 1983, vol. 10, pp. 1–90.
- [13] Semiconductor resource archive, Physical properties of gallium arsenide. [Online]. Available: <http://www.ioffe.rssi.ru/SVA/NSM/Semicond/index.html>.
- [14] A. Othonos, "Probing ultrafast carrier and phonon dynamics in semiconductors," *J. Appl. Phys.*, vol. 83, no. 4, pp. 1789–1830, Feb. 1998.
- [15] Low-temperature-grown MBE GaAs. [Online]. Available: [http://www.eecs.umich.edu/CUOS/posters/pdf/Whitaker\\_thzG\\_LT-GaAs.pdf](http://www.eecs.umich.edu/CUOS/posters/pdf/Whitaker_thzG_LT-GaAs.pdf).
- [16] G. Zhao, R. N. Schouten, N. van der Valk, W. T. Wenckebach, and P. C. M. Planken, "Design and performance of a THz emission and detection setup based on semi-insulating GaAs emitter," *Rev. Sci. Instrum.*, vol. 73, no. 4, pp. 1715–1719, Apr. 2002.
- [17] H. Eisele, M. Naftaly, J. R. Fletcher, D. P. Steenson, and M. R. Stone, "The study of harmonic-mode operation of GaAs TUNNETT diodes and InP Gunn devices using a versatile terahertz interferometer," presented at the 15th Int. Space Terahertz Technology Symp., Northampton, MA, Apr. 27–29, 2004.
- [18] R. Kersting, J. N. Heyman, G. Strasser, and K. Unterrarian, "Coherent plasmons in n-doped GaAs," *Phys. Rev. B, Condens. Matter*, vol. 58, no. 8, pp. 4553–4559, Aug. 1998.
- [19] M. R. Stone, M. Naftaly, N. N. Zinov'ev, and R. E. Miles, "Characteristics of large-aperture photoconductive terahertz antennas," in *Proc. IEEE 10th Int. Terahertz Electronics Conf.*, 2002, pp. 125–128.
- [20] T. Hattori, K. Tukamoto, and H. Nakatsuka, "Time-resolved study of intense terahertz pulses generated by a large-aperture photoconductive antenna," *Jpn. J. Appl. Phys.*, vol. 40, pp. 4907–4912, 2001.
- [21] S.-G. Park, A. M. Weiner, M. R. Melloch, C. W. Siders, J. L. W. Siders, and A. J. Taylor, "High-power narrow-band terahertz generation using large-aperture photoconductors," *IEEE J. Quantum Electron.*, vol. 35, pp. 1257–1267, Aug. 1999.



**Michael R. Stone** (S'00) was born in Leeds, U.K., in 1978. He received the B.Eng. degree in electrical and electronic engineering from The University of Leeds, Leeds, U.K., in 2000, and is currently working toward the Ph.D. degree in electrical and electronic engineering with an emphasis on terahertz technology at The University of Leeds.

His current research interests include the generation and detection of free-space terahertz radiation for pulsed and continuous-wave systems.

**Mira Naftaly**, photograph and biography not available at time of publication.



**Robert E. Miles** (M'82) was born in Kettering, U.K., in 1943. He received the B.Sc. degree from Imperial College London, London, U.K., in 1964, and the External Ph.D. degrees in physics from London University, London, U.K., in 1972, respectively.

From 1964 to 1972, he was a Research Scientist with Zenith Radio Research U.K., London, U.K., where he studied the surface properties of IV–VI compound semiconductors. In 1981, following a period as a Teacher, he joined the Department of Electrical and Electronic Engineering, The University of Leeds, as a Research Engineer. In 1983, he became a Lecturer of electronic engineering with the University of Bradford, and then returned to The University of Leeds in 1985, where he is currently Professor of semiconductor materials and devices and Director of the Institute of Microwaves and Photonics. He has authored or coauthored over 90 journal papers. His interests include terahertz electronics and systems, high-frequency electronic devices, micromachining, and self-organizing molecular systems. He has been a member of numerous European Union (EU) funded research collaborations.

**John R. Fletcher** received the Ph.D. degree from the University of Nottingham, Nottingham, U.K.

He taught at the University of Nottingham for many years. He is a Theoretical Physicist who has specialized in the study of the Jahn–Teller effect and related phenomena. He was a Senior Research Fellow with The University of Leeds, Leeds, U.K. He is currently with the Department of Physics, Durham University, Durham, U.K., where he is involved with novel approaches to the generation and analysis of terahertz frequency radiation.



**David Paul Steenson** (M'96–SM'00) was born in Belfast, Northern Ireland, in 1963. He received the B.Sc. degree (with honors) in electronics and electrical engineering from the University of Manchester, Institute of Science and Technology (UMIST), Manchester, U.K., in 1984, and the Ph.D. degree in physics from the University of Nottingham, Nottingham, U.K., in 1993.

In 1984, he joined Philips Components, Cheshire, U.K., where he was a Microwave Device Development Engineer. In 1986, he joined Philips Research Laboratories, Surrey, U.K., where he was involved with the manufacture, design, and characterization of high-frequency devices in germanium, silicon, and gallium arsenide. In 1989, he joined the Department of Physics, University of Nottingham, where he was involved in the area of high frequency applications of double barrier resonant tunnelling devices (DBRTDs). In 1993, he joined the Department of Electronic and Electrical Engineering, The University of Leeds, Leeds, U.K., as a Research Assistant and continued his research on high-frequency applications of DBRTDs. In 1994, he became a permanent member of the Microwave and Terahertz Technology Group (which later became the Institute of Microwaves and Photonics), The University of Leeds. He is also the Manager of the Wolfson Nanotechnology Cleanroom, The University of Leeds. His research interests are mainly in the field of fabrication and integration of novel millimeter- and submillimeter-wave devices and circuits.

Dr. Steenson is a member of the Institute of Physics (U.K.).